IEEE Access
Multidisciplinary | Rapid Review | Open Access Journal

Received November 29, 2017, accepted January 3, 2018, date of publication January 15, 2018, date of current version March 9, 2018.

Digital Object Identifier 10.1109/ACCESS.2018.2794064

Numerical and Experimental Studies on a Three-Dimensional Numerical Wave Tank

XIAOJIE TIAN[1,2], QINGYANG WANG[1], GUIJIE LIU[1,2], WEI DENG[3], AND ZHIMING GAO[1]

[1]Department of Mechanical and Electrical Engineering, Ocean University of China, Qingdao 266100, China
[2]Key Laboratory of Ocean Engineering of Shangdong Province, Ocean University of China, Qingdao 266100, China
[3]Institute of Oceanographic Instrumentation, Qilu University of Technology, Shandong Academy of Sciences, Qingdao 266100, China

Corresponding author: Guijie Liu (liuguijie@ouc.edu.cn)

This work was supported in part by the National Natural Science Foundation of China under Grant 51609223 and in part by the Projects of Qingdao Application Basic Research under Grant 16-5-1-21-jch.

ABSTRACT A 3-D numerical wave tank (NWT) is proposed in this paper to calculate the wave propagation and hydrodynamics force based on the incompressible Navier–Stokes equations by using the commercial computation fluid dynamics (CFD) software. The volume of fluid method is used to capture free surface. CFD code to generate waves in the NWT is first validated by analytical theory to check its accuracy. Next, a cylinder structure model is introduced to study the interaction of the structure with the wave load. The experiment included a cylinder structure, which was set up in a flume, to compare the wave load against numerical results. The performance of the numerical model is validated and verified by several cases, and it shows very good agreement with the experimental test.

INDEX TERMS Numerical wave tank, computation fluid dynamics, wave-structure interaction, wave load.

I. INTRODUCTION

More and more offshore structures are developed for various purposes, such as offshore platforms, offshore wind turbines, and cage aquaculture. Their structures are under the effect of complex offshore environments, including waves, currents, and wind. In particular, waves are one of the main parameters to consider in the design of structures for offshore environments. The accurate estimation of wave loads are very important for structural design, which is most considered by scholars [1], [2]. Therefore, it is necessary to explore the appropriate wave generating method, which can match the actual marine condition. Now, more and more marine structures appear with the development of ocean resource exploration, which are constructed or supported by cylinder structures. Thus, wave loads on cylinders have been widely studied in coastal and offshore engineering. In 1950, Morison *et al.* [3] put forward the Morison Equation, which can calculate the wave load for the small-scale cylinder strutures. Currently, researchers mainly focus on theoretical analysis, physical model experiments, field observations, and numerical simulation [4]–[6].

The most commonly methods for wave research are physical model experiments in a wave tank or wave flumes, which have been used for decades to conduct tests and research. These tests have provided many valuable results that have helped in the design of devices, structures and even help setup codes. A wave tank is characterized as a long and narrow enclosure with a wave-maker at one end [7]. Waves in the wave tank are generated through the movement of a paddle, which is also known as a wave-maker [8]. The most common of these wave-makers are piston, flap and wedge types. It is apparent that to acquire wave tanks is an expensive task. They also demand a large enough space to house them, which can add to the cost. In addition, prototype construction and testing takes a lot of time. Furthermore, the cost associated with construction of a model at its infant stage is significant, and there is no guarantee that the design would work properly in the first instance. Compounding these expenses is the cost associated with redesign and re-testing.

The need to find an alternative without compromising the integrity of the results has led to the development of Numerical Wave Tanks (NWTs). An NWT is simply a numerical representation of a physical wave tank [9]. The development and advancements in computer processing power have paved the way for the use of Computational Fluid Dynamics (CFD) codes that are used to accomplish this task. Various numerical modeling techniques, such as the boundary element method (BEM), finite element method (FEM) and finite volume method (FVM), are all employed to represent linear wave and nonlinear moving of floating structures in water. Bihs *et al.* [10] developed a three-dimensional NWT to study the wave propagation and calculate the wave loads based on

Navier-Stokes equations. Tutar and Mendi [11] investigated the overall performance of a turbine using the numerical wave flume, which was based on volume of fluid (VOF) method coupled with a finite volume method (FVM) approach. Tang *et al.* [12] investigated the dynamic properties of a dual pontoon floating structure using a two-dimensional fully nonlinear NWT. The boundary element method was used to calculate wave loads. Finnegan and Goggins [13] developed a CFD wave tank model to generate a linear irregular wave for representing real ocean waves at full scale. Hu *et al.* [14] used the CFD package-Open Field Operation and Manipulation to study the interactions of wave and structures. NewWave theory is introduced to establish wave boundary conditions to represent an extreme wave condition. Prasad *et al.* [15] simulated waves in a 3D NWT by employing the VOF method to capture free surface. The numerical code to generate waves in NWT can be verified by experiment data. Li and Lin [16] studied a surface-piercing structure against a combined wave-current flow in a 2-D NWT. The model is based on Reynolds averaged Navier-Stokes (RANS) equations and renormalization group (RNG) k-ε model. Yu and Li [17] employed CFD method based on RANS to investigate the hydrodynamic characteristics of two-body floating-point absorber. Liang *et al.* [18] simulated a piston-type wavemaker to generate a series of irregular wave based on FVM. Moreover, the simulated results were compared to those of an experimental wave tank.

As previously introduced, analytical models are based on many hypotheses, which might show incon-sistency in coupling with the general computational fluid dynamics (CFD) codes. Numerical accuracy and stability are important for the good performance of NWT based on Navier-Stokes equations. NWTs are a promising method for wave research. However, current numerical models for NWTs are still far from mature. Among all the technical difficulties, the accurate generation of waves should be one of the priorities.

In the present work, a 3D NWT is established within a full-scale physical wave tank, which is located at Ocean University of China. Commercial CFD code-Fluent is used to model the 3D NWT. The waves in the NWT is generated using a piston type wave-maker which is located at the inlet of the domain. The CDF code solves the RANS equations and the free-surface is captured using VOF method. Firstly, the numerical code to generate waves in NWT is validated against theoretical solutions to check the accuracy and robustness of the code. Furthermore, a wave-structure interaction model is proposed in the realistic physical wave tank. The use of the numerical model is maximized here as no scaling is introduce, therefore a more realistic model and structure response is presented. And the wave-structure interaction model could be verified by comparing to the experimental results, which can verify the robustness of the 3D NWT code in the meanwhile.

The paper is organized as follows. Section 2 proposed the numerical wave tank. Section 3 established the experimental details of wave and structure interaction. Section 4 discussed the numerical wave tank validation and the numerical results for the interaction of structure with NWT wave. And Section 5 gives the conclusions.

II. NUMERICAL WAVE TANK

A. GOVERNING EQUATIONS

Steady three-dimensional potential flow will be considered in this section, which contains air and water in the computational domain. The two phases are separated by an interface (free surface). The two phase of fluid are both assumed to be incompressible, inviscid and irrational in this study. Also, the two phases are immiscible. Continuity equation and RANS equation are used as the governing equations for the incompressible turbulence fluid. The equations are shown in Equ. (1), (2), (3) and (4) [19]:

$$\frac{\partial u}{\partial x}+\frac{\partial v}{\partial y}+\frac{\partial w}{\partial z}=0 \tag{1}$$

$$\frac{\partial(\rho u)}{\partial t}+\frac{\partial(\rho uu)}{\partial x}+\frac{\partial(\rho uv)}{\partial y}+\frac{\partial(\rho uw)}{\partial z}=-\frac{\partial p}{\partial x}+\mu\left[\frac{\partial^2 u}{\partial x^2}+\frac{\partial^2 u}{\partial y^2}+\frac{\partial^2 u}{\partial z^2}\right]+S_u \tag{2}$$

$$\frac{\partial(\rho v)}{\partial t}+\frac{\partial(\rho vu)}{\partial x}+\frac{\partial(\rho vv)}{\partial y}+\frac{\partial(\rho vw)}{\partial z}=-\frac{\partial p}{\partial y}+v\left[\frac{\partial^2 v}{\partial x^2}+\frac{\partial^2 v}{\partial y^2}+\frac{\partial^2 v}{\partial z^2}\right]+S_v \tag{3}$$

$$\frac{\partial(\rho w)}{\partial t}+\frac{\partial(\rho wu)}{\partial x}+\frac{\partial(\rho wv)}{\partial y}+\frac{\partial(\rho ww)}{\partial z}=-\frac{\partial p}{\partial z}+v\left[\frac{\partial^2 w}{\partial x^2}+\frac{\partial^2 w}{\partial y^2}+\frac{\partial^2 w}{\partial z^2}\right]+S_w \tag{4}$$

Where, x, y, and z represent the coordinate component; u, v, and w are the velocity vector in the x, y, and z directions, ρ is the density, μ is the dynamic viscosity, and Su, Sv, and Sw are the generalized source terms.

The RNG k-ε model was adopted to calculate the results of turbulence phenomena, as shown in Equ. (5) and (6).

$$\frac{\partial(\rho k)}{\partial t}+\frac{\partial(\rho k u_i)}{\partial x_i}=-\frac{\partial}{\partial x_j}\left[\alpha_k \mu_{eff}\frac{\partial k}{\partial x_j}\right]+G_k+\rho\varepsilon \tag{5}$$

$$\frac{\partial(\rho\varepsilon)}{\partial t}+\frac{\partial(\rho\varepsilon u_i)}{\partial x_i}=-\frac{\partial}{\partial x_j}\left[\alpha_\varepsilon \mu_{eff}\frac{\partial \varepsilon}{\partial x_j}\right]+\frac{C_{1\varepsilon}^{*}\varepsilon}{k}G_k-C_{2\varepsilon}\rho\frac{\varepsilon^2}{k} \tag{6}$$

Where K is turbulent energy, ε is turbulent energy dissipation rate, μ_{eff} is diffusion coefficient, G_k is the production of turbulent kinetic energy, and $C_{1\varepsilon}$ and $C_{2\varepsilon}$ are the empirical constants, which are 1.42 and 1.68, respectively.

In the NWT, VOF method is used to capture the fluctuation of the water-air free surface [20]. The coefficient of phase function α is defined as the quantity of water per unit of volume in each domain. This means that if $\alpha = 1$, the whole domain is full of water; if $\alpha = 0$, the whole domain is full of air, and in any other case, it is within the air-water interface. The properties of fluid can be calculated at each

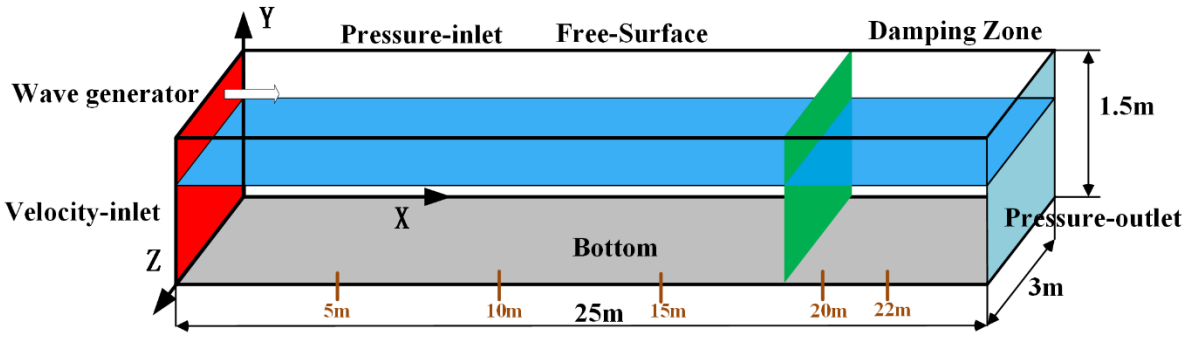

FIGURE 1. Schematic of a 3D numerical wave flume.

section simply by weighting them using VOF function as shown in Equ. (7):

$$\sum_{q=1}^{2} \alpha_q = 1 \tag{7}$$

The continuity equation for the volume fraction is written in Equ. (8):

$$\frac{\partial \alpha_q}{\partial t} + u\frac{\partial \alpha_q}{\partial x} + v\frac{\partial \alpha_q}{\partial y} + w\frac{\partial \alpha_q}{\partial z} = 0 \tag{8}$$

B. NUMERICAL DETAILS

The three-dimensional (3-D) numerical wave flume (NWF) constructed as a representation of the experimental wave flume is illustrated in Fig. 1. The overall size of NWF is 25 m length, 3m width, and 1.5m depth.

Boundary conditions should be set for the computational domain in CFD [21]. There are six boundary conditions in this study, including top, bottom, right, left, front and back, of the 3D numerical wave flume. The boundary condition set is shown in Fig. 1. The no-slip wall condition was imposed on the bottom, front and back boundaries of the numerical tank. Based on the Prantl theory [22], there is a very thin boundary layer near the solid surface. The flow in the boundary layer has great velocity gradient, and the velocity of flow very close to the surface is equal to that of solid surface. The flow velocity outside of boundary layer is uniform and constant, and has no velocity gradient. Therefore, the velocity of flow very close to wall is zero under the no-slip boundary condition. The fluid far away from walls has uniform velocity. The no-slip condition can ensure that the fluid moving over the solid surface does not have a velocity relative to the surface at the point of contact.

The left boundary is defined as the velocity-inlet and the inflow boundary condition was applied by the numerical maker, which was set in a User Defined File (UDF). Top boundary was open to the atmosphere and defined as a pressure-inlet. Thus, the boundary condition was defined as opening with a relative pressure set to 0 Mpa. And the right boundary of computational domain was applied pressure-outlet. The actual boundary conditions are listed in Table 1.

TABLE 1. Boundary conditions.

Boundary	Boundary condition type
left boundary	velocity-inlet
top boundary	pressure-inlet
right boundary	pressure-outlet
front boundary	wall
back boundary	wall
bottom boundary	wall

The propagating waves are produced by a numerical wave generator at the left boundary in the NWT through wave generation domain and the opening absorbing boundary is defined at the right-end boundary to prevent wave reflection back into the flow solution domain. A numerical wave maker was set to reproduce a numerical wave at the inflow boundary by providing the velocity of the numerical wave maker. The velocity vector of the regular wave was defined by the Stokes 2nd order wave theory in this study [23]. The following Equ. (9) and (10) for the velocity components, u_x and u_y, in the x and y directions, respectively are used to generate regular waves at the inflow boundary. η is the wave surface equation, to define the actual wave profile in the inflow boundary, as shown in Equ. (11):

$$u_x = \frac{\pi H}{T}\frac{\cosh k\,(y+d)}{\sinh kd}\cos\left(-\omega t\right) + \frac{3}{4}\frac{\pi H}{T}\frac{\pi H}{L}\frac{\cosh 2k\,(y+d)}{(\sinh kd)^4}\cos 2\left(-\omega t\right) \tag{9}$$

$$u_y = \frac{\pi H}{T}\frac{\sinh k\,(y+d)}{\sinh kd}\sin\left(-\omega t\right) + \frac{3}{4}\frac{\pi H}{T}\frac{\pi H}{L}\frac{\sinh 2k\,(y+d)}{(\sinh kd)^4}\cos 2\left(-\omega t\right) \tag{10}$$

$$\eta = \frac{H}{2}\cos\left(-\omega t\right) + \frac{\pi H}{8}\frac{H}{L}\frac{\cosh kd}{(\sinh kd)^3} \times \left(2+\cosh 2kd\right)\cos 2\left(-\omega t\right) \tag{11}$$

Where H, T, L, and d are the wave height, period, length and water depth, respectively, and their values are 20 cm, 2 s, 5.2 m, and 1 m, respectively, in the NWT.

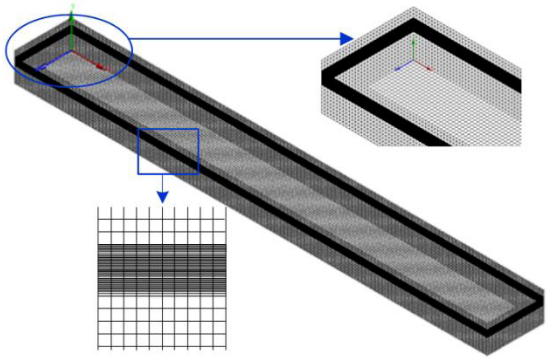

FIGURE 2. 3D NWT model in CFD.

To absorb the wave energy reflecting from the structure wall, end wall and input boundary are set in the NWT. Artificial damping zones are located at a wavelength of the distance from the fluid outlet boundary. In the damping zone, the wave motion also follows the continuity equation. According to the damping term in the momentum equation, wave energy can be absorbed effectively in the damping zone. The momentum equations are shown as follows:

$$\frac{\partial (u)}{\partial t} + u\frac{\partial (u)}{\partial x} + v\frac{\partial (u)}{\partial y} = -\frac{1}{\rho}\frac{\partial p}{\partial x} + v\left[\frac{\partial^2 u}{\partial x^2} + \frac{\partial^2 u}{\partial y^2}\right] - \sigma u \tag{12}$$

$$\frac{\partial (v)}{\partial t} + u\frac{\partial (v)}{\partial x} + v\frac{\partial (v)}{\partial y} = -\frac{1}{\rho}\frac{\partial p}{\partial y} + g_y + v\left[\frac{\partial^2 v}{\partial x^2} + \frac{\partial^2 v}{\partial y^2}\right] - \sigma v \tag{13}$$

$$\sigma (x) = \alpha (x - x_1)(x_2 - x_1) \tag{14}$$

Where σ is the wave damping coefficient, α is the empirical coefficient, and x_1 and x_2 are the starting and end location, respectively, in the damping zone.

The NWT was modeled using commercial CFD code ANSYS-UDF [24]. A finite volume method (FVM)-based numerical flow modeling approach of CFD is used to solve the three-dimensional (3-D), unsteady partial differential equations (continuity, momentum and energy equations) together with the turbulence transport equation, general motion (rotation) of the wave propagation and surface tracking. Within this scheme, pressure and velocity are coupled implicitly by using the time-advanced pressures in the momentum equations and the time advanced velocities in the continuity equations. The NWT model is shown in Fig. 2.

The computational zone is regular, and structural grid is used to mesh. The element size is set at 0.1 m. To accurately capture the wave free surface in real time, the grid is encrypted in a wave higher than the still water. The grid in the wave absorbing zone is gradually thinned by a ratio of 1.2. Thus, Fig. 2 shows the generated multi-block mesh configuration containing the optimum number of 682,500 mesh cells.

III. EXPERIMENTAL TEST

For the purpose of verifying the feasibility of numerical simulation result, a physical model test in wave tank was conducted at the Ocean Engineering Laboratory, at the Ocean University of China. The experiment settings are illustrated in Fig. 3. The wave flume is 3 m wide, 1.5 m deep, and 30 m long, which is equipped with a piston type wave generator at one end to achieve different waves. By controlling the displacement and velocity of the wave generator, desired waves of various heights and periods were obtained. At the other end, a parabolic type passive absorber is installed to absorb the energy of incident wave and minimize wave inflection at the end of the channel. The vertical cylinder model made of polymethyl methacrylate was set 10 m downstream of the wave generator. A capacitance type wave gauge is installed 2.6 m upstream of the vertical cylinder. This gauge is used to measure the incoming wave properties such as wave height (H) and wave period (T). The voltage obtained from the wave gauges are recorded in a computer by using data acquisitions and data monitoring system. Then, the voltages were converted to wave height by calibration. The data sampling rate is taken as 10 units per second for wave measurements. The ranges of wave height and wave period are found to be 0.05-0.2cm and 0.5-2s, respectively. In the experimental test, wave height and wave period are set at 0.2 m, 0.15 m, and 1.5 s, 2.0 s, as shown in Table 2.

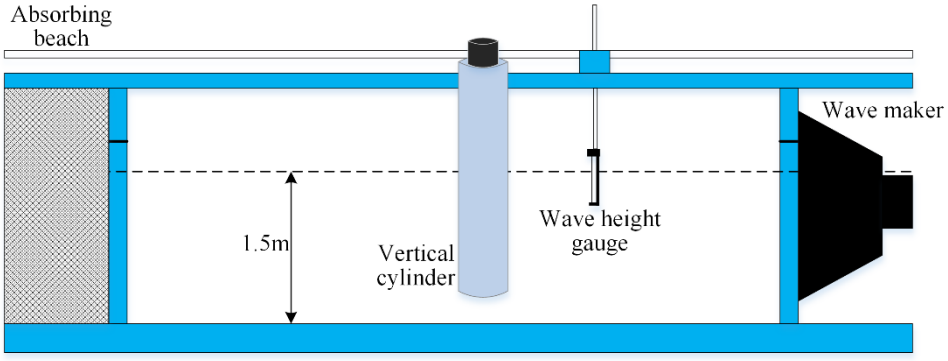

FIGURE 3. Experimental setting of wave flume.

TABLE 2. Experimental wave conditions.

	Wave height H(m)	Wave period T(s)	Wave length(m)
Case 1	0.20	2	6.24
Case 2	0.20	1.5	3.51
Case 3	0.15	1.5	3.51

During the experiment, water depth was set at 1.5 m and the submerged depth was maintained at 1 m. the experimental device is installed as shown in Fig. 4. The experimental device mainly contains a six-dimensional force sensor, metal connection plate, flange and chord pole model.

A fixture structure was installed on the groove wall of the experimental water flume to fix and mount the whole experimental device. The six-dimensional force sensor is on the top, connected to the cylinder model by a chord and a flange. The flange can drive the lower part of mechanism rotation. The wave forces on the vertical cylinder can be measured using the six-dimensional force sensor, which contains three forces and three torques in the directions of x, y, and z, respectively. And the x force is define along the wave propagation as shown in Fig.4, and indicates the wave loads on the cylinder.

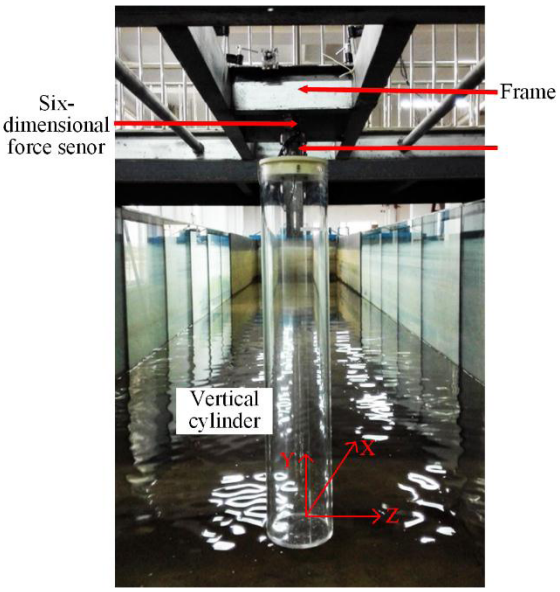

FIGURE 4. Experimental device in the wave flume.

All the digital signal measurement are logged simultaneously and data acquisition was done at 60s intervals with a sampling interval of 0.01 s. 10 wave cycles of data (after wave front) were chosen to measure waves and forces, avoiding possible reflection from the wave absorbing section. The signals of six-dimensional force sensor are handled using a data logger. The voltages were converted to force or torque on the computer that can be recognized directly. The data acquisition system is shown in Fig. 5.

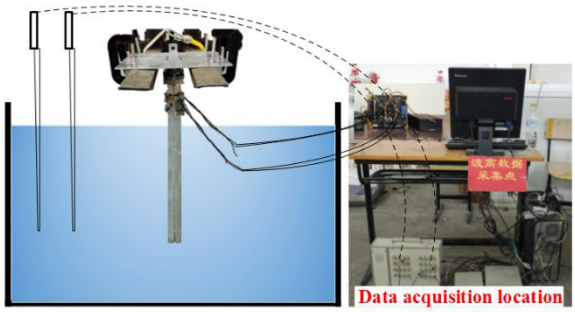

FIGURE 5. Data acquisition system.

IV. RESULTS AND DISCUSSION

A. NUMERICAL WAVE TANK VALIDATION

A series of initial simulations are performed in the NWT. The wave height, wave period, and wave depth are set as 20 cm, 2 s and 1 m, respectively. The formation of the wave travels from left to right as shown in Fig. 6. The wave takes 8 s to reach the back wall and achieves stability at approximately 10s. In Fig. 6, the red region represents water while the blue region represents air. The waveform of the NWT is generated over time and stable after 10 s, when the wave absorbing zone is smooth.

To verify the present numerical approach for modeling of the generation and propagation of regular waves, the wave elevation in NWT is evaluated to compare it to the Stokes 2nd order wave theory. Fig. 7 clearly demonstrates the wave elevation of the numerical data retrieved at a probe position of $x = 5$ m with the analytical theory for the selected medium mesh size of 682,500 mesh cells. Three numerical wave tanks under different wave heights and wave periods are listed in Figure7. At the same time, the incident wave heights were recorded without a structure in the wave flume, which is used to compare with the numerical data. Initially, the wave elevation generated by NWT is smaller than that of the analytical theory and experimental data. But it has been stable after a period of time and correspond well with analytical theory and experimental data under three different cases. Therefore, the validity of using the numerical approach to generate regular waves based on the Stokes Second 2nd order theory was verified.

Five probes have been set at the numerical wave tank to validate the generating wave effect of NWT, including $x = 5$m, $x = 10$m, $x = 15$m, $x = 20$m, and $x = 22$m, as shown in Fig. 1. And the wave elevations at different

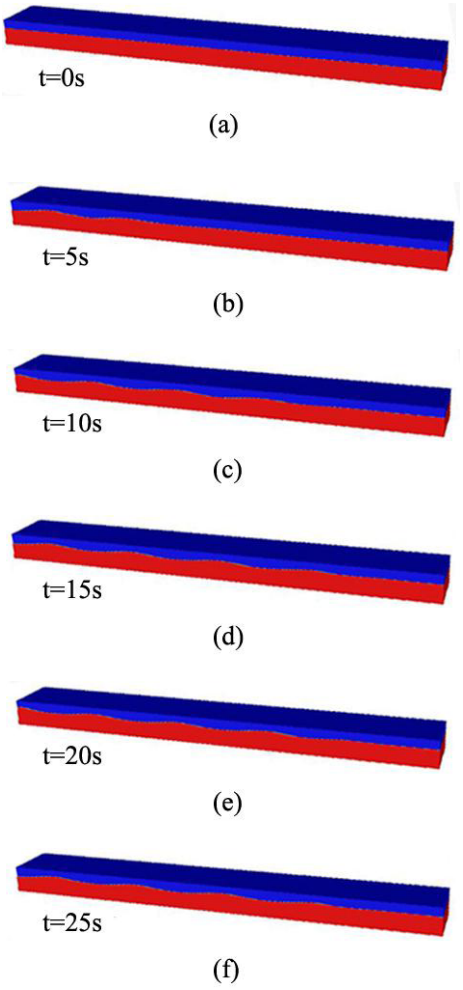

FIGURE 6. Wave propagation in the NWT over time (a) t = 0s, (b) t = 5s, (c) t = 10s, (d) t = 15s, (e) t = 20s, (f) t = 25s.

probe positions are illustrated in Fig. 8. It can be shown that wave heights of 5m, 10m and 15m is very regular over time, which is located at the wave generation zone of numerical tank. However, the wave height becomes smaller when the probe is located at 20m. It is because that the generated wave have been absorbed by the damping zone. When x = 22m, the wave height is always zero over time and the wave height curve is a straight line, which presents no waves here. It also shows that wave energy reflecting from the structure wall have been absorbed completely at the damping zone. It also can be concluded that CFD code for this NWT is validated in the generating zone and damping zone. Moreover, as the wave moving forward, the wave height has a little reduction at x = 10m and x = 15m. This is because that the wave energy decreases as the wave propagation due to the water viscous effect.

B. NUMERICAL RESULTS FOR THE INTERACTION OF STRUCTURE WITH NWT WAVE

A numerical simulation was carried out to investigate the wave loads that affect a cylinder type fixed offshore

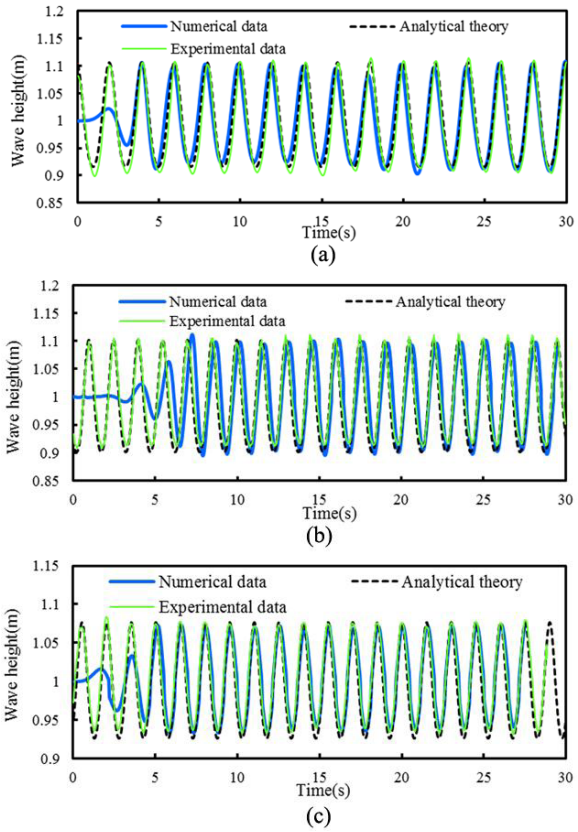

FIGURE 7. Wave elevation history computed at a probe position of x = 5 m for the optimum mesh configuration (a) case 1: H = 0.2 m T = 2 s, (b) case 2: H = 0.2 m T = 1.5 s, (c) case 3: H = 0.15 m T = 1.5 s.

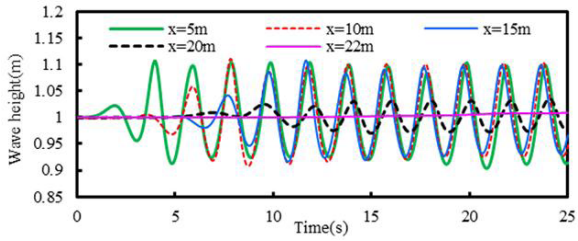

FIGURE 8. Wave elevation history computed at different probe positions in the NWT.

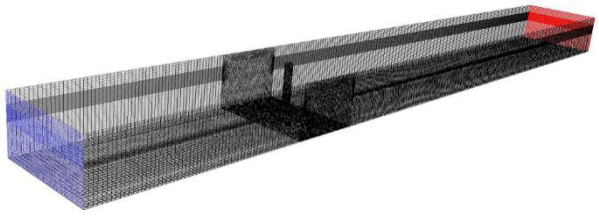

FIGURE 9. Schematic view of the numerical wave tank with a vertical cylinder.

substructure. In this study, a finite long cylinder is adopted to analyze the accuracy of the model's prediction of the interaction of the structure with the NWT wave. The cylinder is positioned 7 meters from the wave maker, as shown in Fig. 9.

The whole NWT model is also mesh with a hexahedral element. It may be noted that additional mesh refinement is needed around the structure because of the introduction of the structure model. The mesh close to the cylinder is used for the tetrahedral element for more refinement. The number of elements in the mesh is increased to 877,790. The wave environment conditions are the same with that of Table 2. A numerical simulation was carried out for a period range as 20 s with three different levels of wave steepness. The condition of the numerical wave maker and damping domain was the same as Figure 2. The total computation time was approximately 24 h with the specification of the computer as an Intel Xenon CPU E5-2640 for the period of a wave.

The interaction between the ocean wave and vertical cylinder is shown in Fig. 10. It illustrates snapshots of the wave surface elevation over a period of time under different wave conditions. These snapshots all illustrate free surface deformations corresponding to the relative vertical cylinder. It can be seen that, the propagation speed of the wave profile is fast in Case 1. The propagation speeds of Case 2 and 3 are nearly the same. This is because the wave velocity is proportional to wave period, and the same wave periods have the same wave velocities. However, the wave profile in Case 3 is inconspicuous because of the small wave height.

By recording the wave displacement at the cylinder face, it can be achieved the effect of a cylinder on the NWT. A wave probe is set at the cylinder face in the NWT, which is at the location of x = 10m. In Fig. 11, the wave displacement with a cylinder in the NWT is compared with that of no cylinder in the NWT. It can be seen that the waveform variation with cylinder is the same with that the NWT. But the maximum value of wave height reduces a lot because of the existence of cylinder.

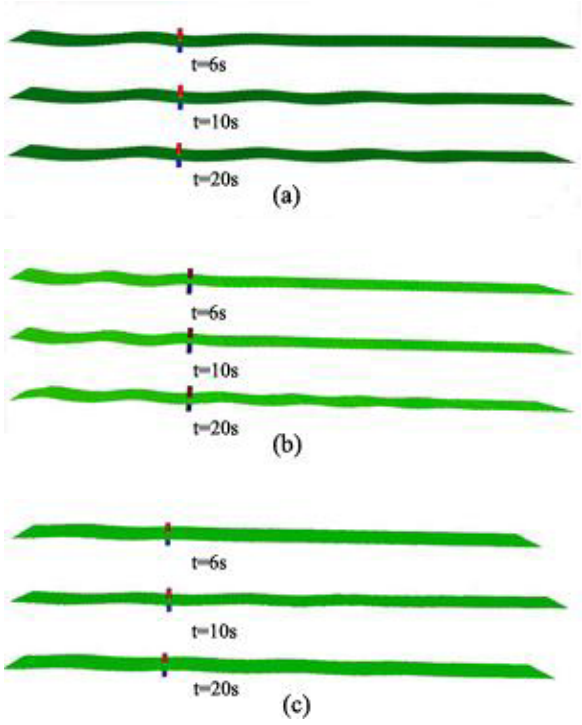

FIGURE 10. Wave profile under different wave conditions (a) case 1: H = 0.2 m T = 2 s, (b) case 2: H = 0.2 m T = 1.5 s, (c) case 3: H = 0.15 m T = 1.5 s.

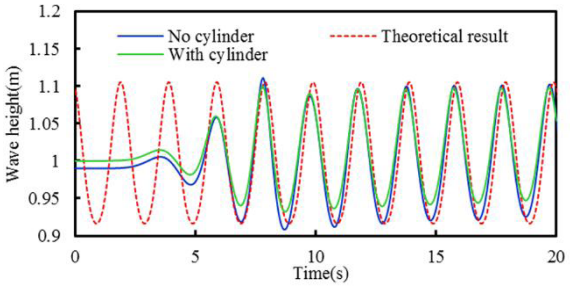

FIGURE 11. Wave height computed at the cylinder face in NWT under case 1 wave conditions.

The total horizontal forces on cylinders were plotted as a function of time, as shown in Fig. 12. Under different wave conditions, the changing trend of wave load on the cylinder is almost the same. The load under Case 2 is almost larger than the other cases. The wave load on the cylinder in the x direction can be written in Equ. (15). It is clear that the wave load is proportional to the velocity in the x direction. u_x is dependent on H/T, as shown in Equ. (15). The value of H/T in Case 2 is larger than in the other cases. Therefore, the wave load obtained by the numerical model is validated and reasonable.

$$F = \frac{1}{2}\rho C_D A u_x^2 + \rho C_M V \dot{u}_x \tag{15}$$

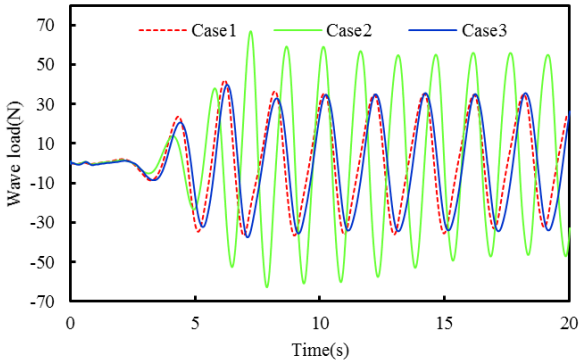

FIGURE 12. Wave load on the vertical cylinder under three wave conditions.

C. COMPARISON OF EXPERIMENTAL RESULTS AND NUMERICAL RESULTS

A comparison between numerical results and experimental results can be seen in Fig. 13. Meanwhile, the theoretical result based on the Morison Equation is used for comparison. The red wave load curve is very regular, which shows the wave load on the vertical cylinder changing theoretically.

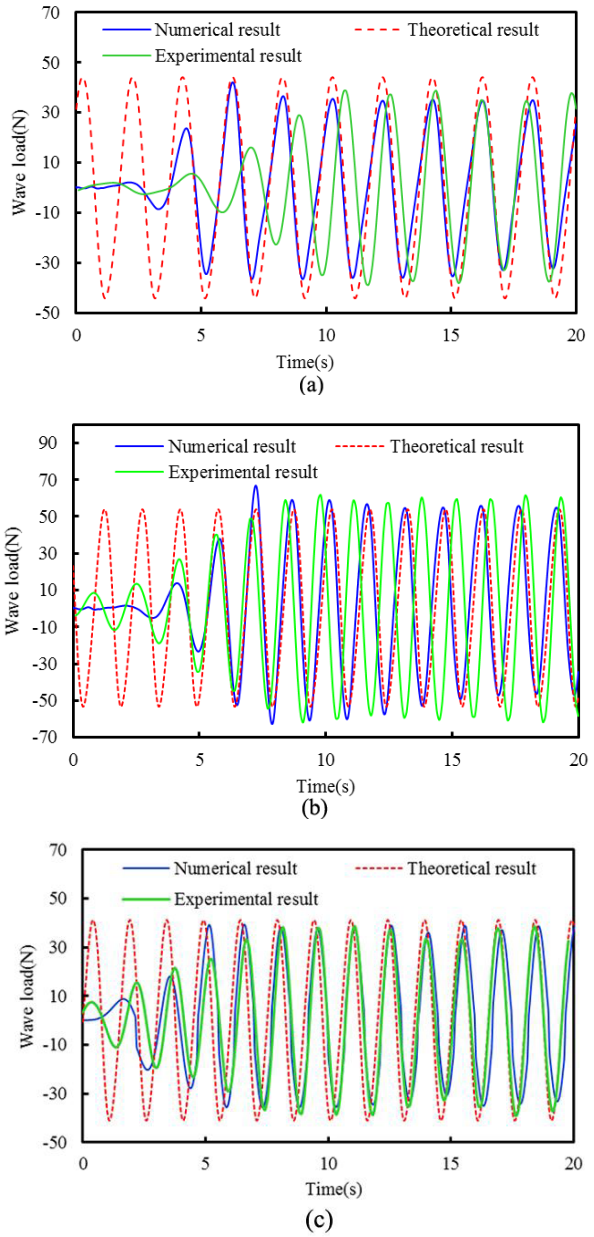

FIGURE 13. Comparison of theoretical result, numerical result and experimental result for wave interaction with a vertical cylinder (a) case 1: H = 0.2 m T = 2 s, (b) case 2: H = 0.2 m T = 1.5 s, (c) case 3: H = 0.15 m T = 1.5 s.

At the initial time, numerical results and experimental results both increases with the time and reaches a stable state after a period of time. For Case 1, the numerical wave tank takes about 5s to reach stable. So the wave load curve is changing similar to the theoretical result. For experimental result, its period has a little difference with other results, but the magnitude of load is almost same with numerical result. For Case 2, the load magnitude of numerical and experimental results are almost same with theoretical result. But the period of experimental data is smaller. For Case 3, numerical result is consistency with the theoretical result. But the experimental result have a little differences. It can be concluded that numerical results have good consistency with the theoretical results, and have a little differences with the experimental results. It can be explained that the experimental results may be affected by the factors of measurement equipment, cylinder structures, and environment and so on. Therefore, the numerical results are in an ideal condition, which is very close to the theory results. It also shows that the NWT is validated to simulate different wave conditions and can be extended to the model.

V. CONCLUSION

In the work, a numerical model for a wave tank that can accurately simulate ocean wave is proposed. The incompressible Navier-Stokes equations are used to solve with RANS turbulence closure. To obtain stable and accurate wave propagation results, high-order numerical discretization schemes on a Cartesian mesh are chosen. Next, the interactions of wave with a vertical cylinder are studied computationally for different wave heights and wave periods. Meanwhile, a physical model test was conducted in a wave flume to verify the feasibility of the numerical simulation result. The following can be concluded:

(1) The presented numerical wave tank has been validated by analytical theory based on Stokes Second 2nd order wave theory.

(2) Comparisons between experimental test and numerical results showed good agreement. The submerged cylinder case also revealed that the NWT has the capability to accurately predict wave load and wave transformation.

(3) It is clear from this analysis that actual ocean wave conditions can be modeled accurately by NWT method, which has low price in comparison with physical model testing.

(4) Moreover, the established numerical modeling can be maximized by adopting full scale measured data and replicating it in a full-scale NWT.

REFERENCES

[1] S.-K. Lee, D. Yan, B. Zhang, and C. Kang, "Jack-up leg hydrodynamic load prediction—A comparative study of industry practice with CFD and model test results," in *Proc. 9th Int. Offshore Polar Eng. Conf.*, Osaka, Japan, 2009, pp. 1–8.

[2] C. Lopez-Pavon and A. Souto-Iglesias, "Hydrodynamic coefficients and pressure loads on heave plates for semi-submersible floating offshore wind turbines: A comparative analysis using large scale models," *Renew. Energy*, vol. 81, pp. 864–881, Sep. 2015.

[3] J. R. Morison, J. W. Johnson, and S. A. Schaaf, "The force exerted by surface waves on piles," *J. Petroleum Technol.*, vol. 189, pp. 149–154, May 1950.

[4] J. Maljaars, R. J. Labeur, M. Möller, and W. Uijttewaal, "A numerical wave tank using a hybrid particle-mesh approach," *Procedia Eng.*, vol. 175, pp. 21–28, Jan. 2017.

[5] L. Xiao, J. Yang, T. Peng, and L. Tao, "A free surface interpolation approach for rapid simulation of short waves in meshless numerical wave tank based on the radial basis function," *J. Comput. Phys.*, vol. 307, pp. 203–224, Feb. 2016.

[6] S. Ganesan and D. Sen, "Direct time domain analysis of floating structures with linear and nonlinear mooring stiffness in a 3D numerical wave tank," *Appl. Ocean Res.*, vol. 51, pp. 153–170, Jun. 2015.

[7] G. T. Shivaji and D. Sen, "A 3D numerical wave tank study for offshore structures with linear and nonlinear mooring," *Aquatic Procedia*, vol. 4, pp. 492–499, Jul. 2015.
[8] S. Saincher and J. Banerjeea, "Design of a numerical wave tank and wave flume for low steepness waves in deep and intermediate water," *Procedia Eng.*, vol. 116, pp. 221–228, Jan. 2015.
[9] S.-Y. Kim, K.-M. Kim, J.-C. Park, G.-M. Jeon, and H.-H. Chun, "Numerical simulation of wave and current interaction with a fixed offshore substructure," *Int. J. Naval Archit. Ocean Eng.*, vol. 8, no. 2, pp. 188–197, 2016.
[10] H. Bihs, A. Kamath, M. A. Chella, A. Aggarwal, and O. A. Arntsen, "A new level set numerical wave tank with improved density interpolation for complex wave hydrodynamics," *Comput. Fluids*, vol. 140, pp. 191–208, Nov. 2016.
[11] M. Tutar and M. Mendi, "A performance study of a horizontal-axis microturbine in a numerical wave flume," *Energy Procedia*, vol. 112, pp. 83–91, Mar. 2017.
[12] H.-J. Tang, C.-C. Huang, and W.-M. Chen, "Dynamics of dual pontoon floating structure for cage aquaculture in a two-dimensional numerical wave tank," *J. Fluids Struct.*, vol. 27, no. 7, pp. 918–936, 2011.
[13] W. Finnegan and J. Goggins, "Linear irregular wave generation in a numerical wave tank," *Appl. Ocean Res.*, vol. 52, pp. 188–200, Aug. 2015.
[14] Z. Z. Hu, D. Greaves, and A. Raby, "Numerical wave tank study of extreme waves and wave-structure interaction using OpenFoam," *Ocean Eng.*, vol. 126, pp. 329–342, Nov. 2016.
[15] D. D. Prasad, M. R. Ahmed, Y.-H. Lee, and R. N. Sharma, "Validation of a piston type wave-maker using Numerical Wave Tank," *Ocean Eng.*, vol. 131, pp. 57–67, Feb. 2017.
[16] Y. Li and M. Lin, "Wave-current impacts on surface-piercing structure based on a fully nonlinear numerical tank," *J. Hydrodyn. B*, vol. 27, no. 1, pp. 131–140, 2015.
[17] Y.-H. Yu and Y. Li, "Reynolds-averaged Navier–Stokes simulation of the heave performance of a two-body floating-point absorber wave energy system," *Comput. Fluids*, vol. 73, pp. 104–114, Mar. 2013.
[18] X.-F. Liang, J.-M. Yang, J. Li, L.-F. Xiao, and X. Li, "Numerical simulation of irregular wave-simulating irregular wave train," *J. Hydrodyn. B*, vol. 22, no. 4, pp. 537–545, 2010.
[19] F. Wang, *Computational Fluid Dynamics Analysis*. Beijing, China: Tsinghua Univ. Press, 2004.
[20] Y. M. Shen, C. O. Ng, and Y. H. Zheng, "Simulation of wave propagation over a submerged bar using the VOF method with a two-equation k–ε turbulence modeling," *Ocean Eng.*, vol. 31, no. 1, pp. 87–95, 2004.
[21] G. S. Beavers and D. D. Joseph, "Boundary conditions at a naturally permeable wall," *J. Fluid Mech.*, vol. 30, pp. 197–207, Oct. 1967.
[22] H. J. H. Clercx and C.-H. Bruneau, "The normal and oblique collision of a dipole with a no-slip boundary," *Comput. Fluids*, vol. 35, no. 3, pp. 245–279, 2006.
[23] G. L. Logvinovich, *Hydrodynamics of Free Boundary Flows*. Shanghai, China: Shanghai Jiaotong Univ. Press, 1973.
[24] *Ansys Fluent 14.5*, ANSYS Fluent User's Guide. Inc., Canonsburg, PA, USA, 2012.

XIAOJIE TIAN received the B.S. degree in mechanical design, manufacturing and automation and the Ph.D. degree in mechanical and electronic engineering from the China University of Petroleum in 2008 and 2014, respectively. She is currently a Lecturer with the Ocean University of China. Her research interests include ocean platform structure, computational simulation, and structure optimal design.

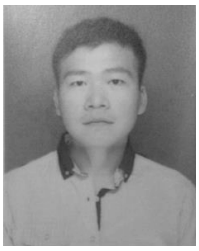

QINGYANG WANG received the B.S. degree in mechanical design, manufacturing and automation from the Henan University of Science and Technology in 2016. He is currently pursuing the M.S. degree with the College of Mechanical and Electronic Engineering, Ocean University of China. His current research interests include ocean platform structure and structure optimal design.

GUIJIE LIU received the Ph.D. degree in mechanical and electronic engineering from Northeastern University in 2004. He is currently with the Department of Mechanical and Electrical Engineering, Ocean University of China, Qingdao, China. His current research interests include ocean platform structure and underwater robots.

WEI DENG received the B.S. degree in mechanical design, manufacturing and automation from the China University of Petroleum in 2008 and the Ph.D. degree in mechanical and electronic engineering from the PLA University of Science and Technology in 2014. He is currently with the Institute of Oceanographic Instrumentation, Shandong Academy of Sciences, Qingdao, China.

ZHIMING GAO received the B.S. degree in mechanical design, manufacturing and automation from the Qilu University of Technology in 2015. He is currently pursuing the M.S. degree with the College of Mechanical and Electronic Engineering, Ocean University of China. His current research interests include ocean platform structure and wave-current computational simulation.